ISSN 1070-4272, Russian Journal of Applied Chemistry, 2017, Vol. 90, No. 12, pp. 1944−1952. © Pleiades Publishing, Ltd., 2017.
Original Russian Text © A.A. Nepomnyashchiy, E.A. Buluchevskiy, A.V. Lavrenov, V.L. Yurpalov, T.I. Gulyaeva, N.N. Leont'eva, V.P. Talzi, 2017, published in Zhurnal Prikladnoi Khimii, 2017, Vol. 90, No. 11, pp. 1613−1622.

CATALYSIS

Hydrodeoxygenation of Vegetable Oil on $NiMoS/WO_3–Al_2O_3$ Catalysts

A. A. Nepomnyashchiy[a,*], E. A. Buluchevskiy[a,b], A. V. Lavrenov[a], V. L. Yurpalov[a], T. I. Gulyaeva[a], N. N. Leont'eva[a], and V. P. Talzi[a]

[a] *Institute of Hydrocarbons Processing, Siberian Branch, Russian Academy of Sciences, ul. Neftezavodskaya 54, Omsk, 644040 Russia*
[b] *Omsk F.M. Dostoevsky State University, ul. Neftezavodskaya 11, Omsk, 644053 Russia*
**e-mail: himik@ihcp.ru*

Received November 7, 2017

Abstract—Tungstate-containing aluminum oxide is suitable as a catalyst support for hydrodeoxygenation of sunflower oil, ensuring 81–83 wt % yield of liquid products at 380°C, 4.0 MPa, and feed space velocity of 1 h^{-1}. The catalyst acidity increases with increasing tungsten oxide content, leading to an increase in the content of decarboxylation/decarbonylation products and isoparaffins in the product mixture.

DOI: 10.1134/S1070427217120084

Hydrodeoxygenation of various vegetable and animal fats is today one of the most popular pathway of processing renewable raw materials [1–3]. This process allows production of environmentally clean fuels identical in their motor characteristics to traditional petroleum diesel fuels or even surpassing them. The carbon dioxide emissions in combustion of such fuels are not taken into account within the framework of the Kyoto Protocol. The hydrodeoxygenation products are mixtures of C_{15}–C_{18} hydrocarbons and can be used in internal combustion engines both in the straight form and in a mixture with a traditional petroleum fuel.

The following systems have been tested as hydrodeoxygenation catalysts: supported noble metals (Pt, Pd, Ru, etc.) [4–7], mono- and bimetal systems based on Co, Ni, and Mo [8, 9], and also traditional Ni(Co)–Mo(W) petroleum fuel hydrotreating catalysts in the oxide [10–14] or sulfide [6, 15–20] form. Catalysts of the latter type are mentioned in research papers most frequently; they are also used in the known industrial processes for hydrodeoxygenation of oil-and-fat raw materials such as NexBTL (Neste Oil) [21] and Ecofining (UOP) [22].

According to the modern views, hydrodeoxygenation of fats on hydrotreating catalysts occurs in several steps. The first step involves hydrogenation of C=C double bonds in fatty acid residues. As a result of hydrolysis and hydrogenolysis, triglycerides decompose with the release of free fatty acids and propane. Then, the fatty acids are hydrogenated to aldehydes. The conversion of aldehydes to hydrocarbons can occur along two pathways: hydrogenation to alcohol, followed by dehydration/hydrogenation and formation of a hydrocarbon with the same number of carbon atoms as in the initial molecule, or β-elimination with the release of CO and formation of a hydrocarbon with the number of carbon atoms smaller by unity than in the initial acid. The occurrence of the second pathway can be favored by increased basicity (electron density) on atoms that can act as an electron pair donors in interaction with hydrogen, e.g., on S^{2-} anions [23, 24]. For example, as shown in [9, 16, 25, 26], introduction of H_2S or another unstable sulfur-containing compound into the reaction medium, usually done with the aim of stabilizing the composition of sulfide phases in the catalyst, increases the decarbonylation/decarboxylation rate; as a result, the yield of hydrocarbons with an odd number of carbon atoms increases.

The kind of support strongly influences the properties of fat hydrodeoxygenation catalysts. The majority of authors note that the support participates in hydrolysis of fatty acid triglycerides and in secondary transformations of the *n*-alkanes formed: isomerization and cracking.

In addition, the support acidity influences the pathway of the transformation of fatty acids into final products. For example, an increase in the total acidity determined by temperature-programmed ammonia desorption and in the Brønsted acidity correlates with an increase in the C_{n-1}/C_n hydrocarbon ratio in reaction products (where n is the number of carbon atoms in the initial fatty acid), which suggests predominant occurrence of decarbonylation/decarboxylation in the course of hydrodeoxygenation of fatty acids [27, 28]. The most widely used support is Al_2O_3 [29]. We also studied SiO_2 [30], amorphous aluminosilicate [31], carbon supports [7, 8, 32, 33], TiO_2 [34, 35], ZrO_2 [14, 27, 36, 37], zeolites (SBA-15 [28, 38], MCM-41 [39], ZSM [40], SAPO-11 [5, 41–43], and their mixtures [44, 45]), and anion-modified metal oxides, in particular, B_2O_3–Al_2O_3 [46, 47].

As a rule, fat deoxygenation products obtained on traditional hydrotreating catalysts contain large amounts of *n*-alkanes. Therefore, they have high congealing points and are unsuitable as winter diesel fuels [48]. To improve the low-temperature characteristics, such fuels are additionally subjected to isomerization dewaxing on zeolite-containing catalysts with supported noble metals [21, 49–51]. The use of a two-step processing scheme makes the process considerably more expensive and decreases the yield of liquid products. Attempts to combine the hydrodeoxygenation and isomerization in one process were made in [52–55] using metals supported on zeolites. Although these systems showed high initial activity, they underwent rapid deactivation.

In this study, we examined the NiMoS/WO_3–Al_2O_3 system as a fat hydrodeoxygenation catalyst to obtain a product with increased isoalkane content. We studied the influence exerted by the composition and properties of the WO_3–Al_2O_3 support on the activity and stability of nickel–molybdenum catalysts for vegetable oil hydrodeoxygenation and on the yield and composition of the products.

EXPERIMENTAL

Catalyst preparation. Tungsten-containing supports WO_3–Al_2O_3 (WA) were prepared by mixing commercial pseudoboehmite (Industrial Catalysts, Ryazan, Russia) with aqueous solutions of ammonium metatungstate (analytically pure grade, Fluka), followed by drying (120°C, 12 h) and calcination (750°C, 4 h). The nominal content of tungsten oxide in the catalysts was varied from 5 to 30 wt % (samples WA-5–WA-30) by using ammonium metatungstate solutions of different concentrations.

The catalysts were prepared by impregnating the support (fraction 0.2–0.5 mm) with solutions of nickel–molybdenum bimetal citrate complexes in a vacuum. The impregnation solutions were prepared using citric acid [GOST (State Standard) 908–04, Reakhim], $(NH_4)_6Mo_7O_{24}\cdot 4H_2O$ (OOO TsT Lantan), and $Ni(CH_3COO)_2\cdot 4H_2O$ (chemically pure grade, Reakhim). The solution concentration was chosen so as to obtain 3.6 wt % Ni and 11.0 wt % Mo content of the ready catalyst. After the impregnation completion, the samples were dried at 220°C for 2 h.

Methods for studying supports and catalysts. The tungsten content of the supports was determined gravimetrically. The nickel and molybdenum content of the catalysts was determined by inductively coupled plasma atomic emission spectrometry with a Varian 710-ES spectrometer (Agilent Technologies).

The phase composition of the supports was determined by X-ray diffraction analysis with a D8 Advance powder X-ray diffractometer (Bruker) using CuK_α radiation (λ = 0.15406 nm) and a Lynxeye position-sensitive detector. The diffraction patterns were interpreted using the ICDD PDF-2 powder diffraction database (2006) and the EVA program (Bruker). The unit cell parameters were refined using the TOPAS 4.2 program (Bruker) by the least-squares method. The coherent scattering domain (CSD) size was calculated by the method of fundamental parameters (FP) taking into account the instrumental error.

The texture characteristics of the supports (S_{sp}, specific surface area; V_{ads}, specific pore volume; D_m, mean pore diameter) were determined by low-temperature nitrogen adsorption using an ASAP 2020 volumetric vacuum static installation (Micromeritics). The BET specific surface area (S_{sp}) was calculated from the adsorption isotherm at relative nitrogen vapor pressures in the interval 0.05–0.30. The specific adsorption pore volume (V_{ads}) was determined from the nitrogen adsorption at an equilibrium relative nitrogen vapor pressure of 0.990. The mean pore diameter (D_m) was determined as the ratio $4V_{ads}/S_{sp}$.

The total acidity of support samples was determined by temperature-programmed desorption (TPD) of ammonia in the temperature range 100–550°C (AutoChem-2920, Micromeritics). A 10 vol % NH_3–He

mixture was used in TPD experiments. The ammonia adsorption was performed at 100°C for 60 min. Weakly bound ammonia was removed by purging with helium at 100°C for 60 min. The desorption was performed in the temperature range 100–550°C. The measurement cell with the sample was heated at a rate of 10 deg min^{-1}. To reach the baseline, the sample was kept at 550°C for 30 to 60 min.

The acid properties of the supports and catalysts were also studied by ESR spectroscopy of perylene probe molecules [56]. Prior to spectroscopic studies, the samples were preliminarily activated by calcination of a series of weighed portions in air in quartz ampules at 750°C and, after cooling to 25°C in a desiccator, were treated with a solution of perylene in hexane (2×10^{-3} M). The suspensions obtained were allowed to stand for 1–40 h, after which the ESR spectra of the radical cations formed were recorded, and the concentration of these species was determined by double numerical integration of the signal. ESR measurements were performed at 25°C with a Bruker EMXplus spectrometer operating in the X-range (9.7 GHz) with the ER 4105 DR cavity at the microwave radiation power of 2.0 mW, modulation frequency of 100 kHz, and modulation amplitude of 0.3 G. Quantitative analysis was performed using references for ESR spectroscopy based on ultradispersed diamond (UDD) with the number of spins 1.44×10^{16}. The ESR spectra were processed using the WinEPR Processing program.

Analysis of the raw material composition. Hydrodeoxygenation experiments were performed with refined sunflower oil produced by the Yug Rusi Plant (Russia). The qualitative and quantitative composition of the oil was determined according to GOST (State Standard) 30418–96. The ester interchange of the oil was performed with an alcoholic solution of sodium ethylate. The obtained mixture of fatty acid ethyl esters was analyzed by gas–liquid chromatography (Agilent HP-5ms column, 30 m). The components were identified with a mass-spectrometric detector. The quantitative composition of the sample was determined with a flame ionization detector by the normalization method.

Catalyst tests. Hydrodeoxygenation of vegetable oil was performed in a flow-through reactor with a fixed catalyst bed. Prior to the tests, the catalysts were dried in a hydrogen stream (300 mL min^{-1}) at 120°C for 5 h and sulfidized in two steps at 230 and 340°C at the heating rate of 25 deg h^{-1}, feed space velocity of 2 h^{-1}, and H_2/feed ratio of 300 $m^3_{n.c.}$ m^{-3}. As a sulfudizing agent we used a solution of dimethyl disulfide in straight-run naphtha (0.6 wt % in terms of S).

Hydrodeoxygenation of sunflower oil was performed at 380°C, pressure of 4.0 MPa, feed space velocity of 1 h^{-1}, and H_2/oil ratio of 2500 $m^3_{n.c.}$ m^{-3}. Hydrogen sulfide was additionally introduced into the reaction mixture in an amount of 0.4% of the hydrogen volume fed.

Product analysis. Samples of liquid and gaseous hydrodeoxygenation products separated in a separator at atmospheric pressure and 20°C were taken at 4-h intervals in the first 24 h and then at 24-h intervals. All the catalysts were run for 150 h. The composition of gaseous products was determined on-line using a Khromos GKh-1000 two-channel gas chromatograph. Inorganic components of the gas phase (H_2, H_2S, CO, CO_2, and H_2O) were analyzed using two columns (3 m × 4 mm) packed with Porapak R and activated charcoal in combination with a thermal conductivity detector. The hydrocarbon components of the gas phase (C_1–C_4, C_{5+}) were analyzed using a capillary column (Agilent DB-1, 60 m) and a flame-ionization detector.

The hydrocarbon composition of the stable liquid product was determined with a Khromos GKh-1000 chromatograph equipped with a capillary column (Restek Rtx-1, 105 m) and a flame ionization detector. To determine the degree of the oxygen removal and to estimate the group composition of the products obtained, the liquid hydrocarbon product was also analyzed by ^1H and ^{13}C NMR spectroscopy with a Bruker Avance 400 spectrometer (400 MHz).

RESULTS AND DISCUSSION

Raw material composition. The raw material composition determined according to GOST (State Standard) 30418–96 is given in Table 1. As can be seen, the raw material contains (in terms of acids) 92.5% C_{18} acids and 6.4% C_{16} acids. The total content of unsaturated acids (mainly oleic and linoleic) is 89.4%.

Composition and physicochemical characteristics of supports and catalysts. Data on the actual chemical composition and on textural and structural characteristics of the supports and catalysts are given in Table 2. As can be seen, the actual content of Ni, Mo, and W in the samples agrees with the calculated values.

A study of the textural characteristics of the support samples has shown that WA supports are mesoporous materials with the mean pore size of 8.5–11.4 nm and pore volume of 0.3–0.5 $cm^3\ g^{-1}$. Such textural characteristics are typical of γ-alumina. On introducing 4.8 wt % tungsten oxide into the support, its specific pore volume increases from 0.40 to 0.49 $cm^3\ g^{-1}$, and the specific surface area, from 145 to 170 $m^2\ g^{-1}$. The mean pore diameter changes insignificantly. Further increase in the modifier content leads to a decrease in V_{ads} and D_m. The specific surface area increases up to 11.6 wt % WO_3 content, and at higher WO_3 content it decreases. However, even for the samples containing 25–30 wt % WO_3 the specific surface area is close to that of the initial alumina and amounts to 141–148 $m^2\ g^{-1}$.

The X-ray diffraction patterns of support samples with the WO_3 content of up to 25 wt % contain only the reflections characteristic of the γ-Al_2O_3 phase, and the reflections of the separate WO_3 phase appear only in X-ray diffraction pattern of the WA-30 sample (Fig. 1). This WO_3 has monoclinic lattice (space group $P2_1/a$) and is designated in the literature as α-WO_3 [57]. The crystallite (CSD) size of the γ-Al_2O_3 phase does not significantly vary throughout the sample series.

The calculated unit cell parameters of γ-Al_2O_3 increase with an increase in the WO_3 content from 7.917 Å for WA-5 to 7.924 Å for WA-30. This may be due to partial incorporation of W^{6+} ions into the aluminum oxide structure. The Shannon ionic radius of W^{6+} (IR = 0.60 Å) is larger than that of Al^{3+} (IR = 0.535 Å) [58]. As a result, the unit cell parameters increase.

Table 1. Fatty acid composition of refined sunflower oil

Acid	Acid weight fraction, wt %
Tetradecanoic (myristic) (C14:0)	0.05
Hexadecanoic (palmitic) (C16:0)	6.30
Hexadecenoic (palmitoleic) (C16:1)	0.07
Octadecanoic (stearic) (C18:0)	3.20
Octadecenoic (oleic) (C18:1)	25.70
Octadecadienoic (linoleic) (C18:2)	63.50
Eicosanoic (arachidic) (C20:0)	0.29
Docosanoic (begenic) (C22:0)	0.79

Acidity of supports and catalysts. The strength and concentration of acid sites in the support samples were evaluated from the ammonia TPD data. The acid sites are subdivided into weak (up to 250°C), medium (250–350°C), and strong (350–550°C), according to [59]. The strength distribution of the acid sites is given in Table 3. As can be seen, modification of aluminum oxide with tungsten oxide leads to a certain increase in the total acidity of the supports. On the other hand, the surface density of the acid sites does not noticeably change compared to pure aluminum oxide and is 2.5–2.8 μmol m^{-2} for all the samples except WA-30. The increase in the total acidity, observed as the WO_3 content is increased from 0 to 25.3 wt %, correlates with an increase in the

Table 2. Chemical composition and textural and structural characteristics of the samples

Sample	Content of elements, wt %			Textural and structural characteristics of supports			
	Ni	Mo	WO_3[a]	S_{sp}, $m^2\ g^{-1}$	V_{ads}, $cm^3\ g^{-1}$	D_m, nm	Al_2O_2 CSD size, nm
NiMo/WA-0	3.7	11.9	–	145	0.40	11.0	5.8
NiMo/WA-5	3.8	12.0	4.8	170	0.49	11.4	6.1
NiMo/WA-10	3.7	12.1	11.6	179	0.44	9.9	6.3
NiMo/WA-15	3.6	12.2	16.1	173	0.43	9.8	6.3
NiMo/WA-20	3.7	12.0	21.2	161	0.39	9.8	6.4
NiMo/WA-25	3.7	12.2	25.3	148	0.33	8.9	6.5
NiMo/WA-30	4.1	12.4	30.1	141	0.29	8.5	6.6

[a] WO_3 content of the support.

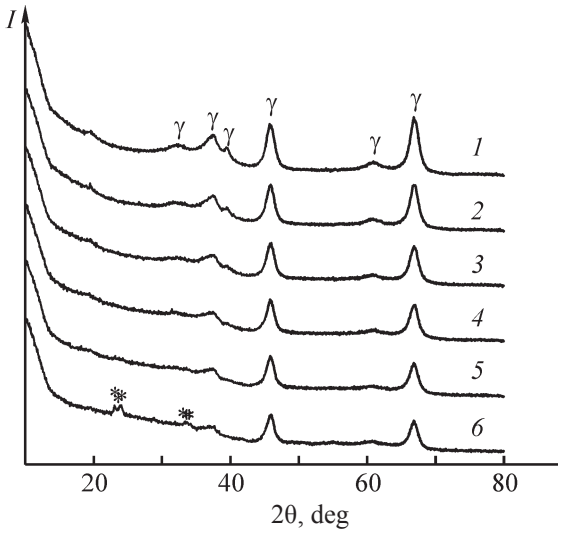

Fig. 1. X-ray diffraction patterns of support samples: (*1*) WA-5, (*2*) WA-10, (*3*) WA-15, (*4*) WA-20, (*5*) WA-25, and (*6*) WA-30. Peks: (*) WO_3 and (γ) γ-Al_2O_3. (*I*) Intensity and (2θ) Bragg angle.

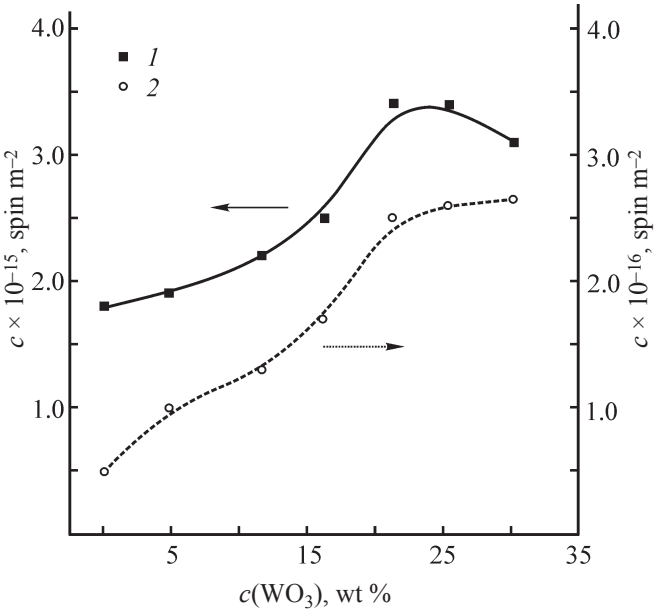

Fig. 2. Concentration c of perylene radical cations per unit surface area for the support and catalyst as a function of the WO_3 content, $c(WO_3)$, of the support. (*1*) Catalyst and (*2*) support.

specific surface area of the samples. The WA-30 sample exhibits somewhat higher surface density of acid sites and lies out of this relationship, which may be due to the presence of the free α-WO_3 phase.

Introduction of tungsten oxide into the supports significantly alters the strength distribution of acid sites: The fraction of strong sites decreases from 41 to 22–27%, and the fraction of medium and weak sites increases from 23 to 28–32% and from 37 to 41–46%, respectively.

The acid properties of supports and catalysts were additionally evaluated by ESR spectroscopy using perylene as a probe. Figure 2 shows how the concentration of perylene radical cations formed on unit surface area of the support and catalyst samples depends on the tungsten oxide content. The concentration of radical cations determining, according to [56], the sum of weak, medium, and strong Brønsted acid sites (BASs) increases in the WO_3 concentration interval 0–30.1 wt %. For the catalysts, the trend observed in going from NiMo/WA-0

Table 3. Acid properties of supports, according to temperature-programmed ammonia desorption data

Sample	T_{max}, °C,	NH_3 desorption		Fraction of ammonia desorbed in indicated interval		
		μmol g^{-1}	μmol m^{-2}	up to 250°C	250–350°C	350–550°C
WA-0	196; 393	375	2.6	0.37	0.23	0.41
WA-5	189; 377	425	2.5	0.44	0.29	0.27
WA-10	189; 315	475	2.7	0.41	0.28	0.31
WA-15	189; 292	458	2.7	0.44	0.29	0.27
WA-20	185; 234	452	2.8	0.44	0.32	0.24
WA-25	185; 255	410	2.8	0.44	0.32	0.23
WA-30	200	439	3.1	0.46	0.32	0.22

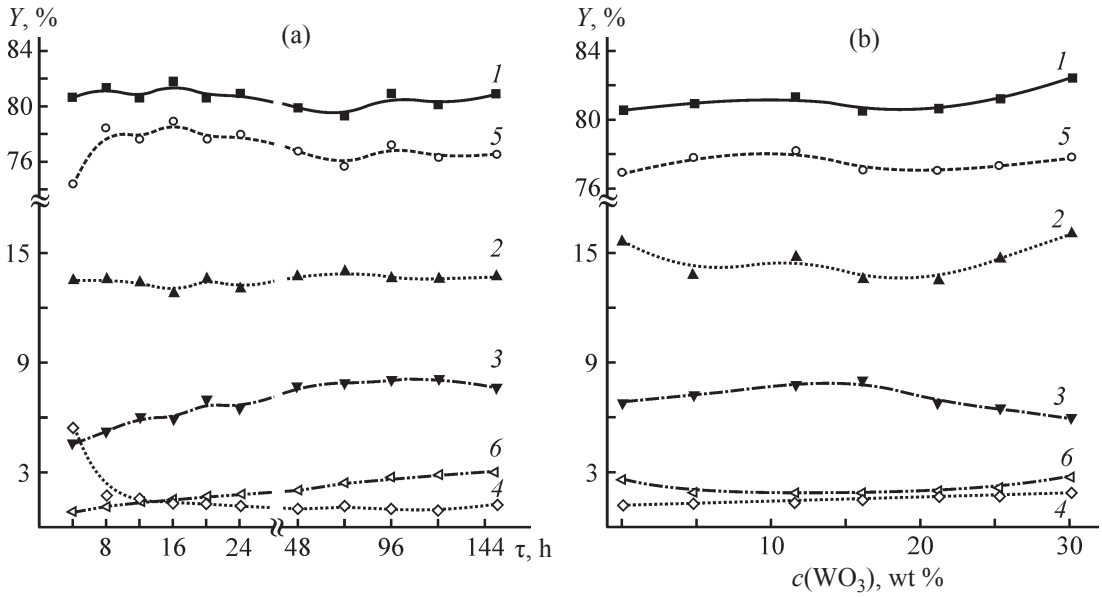

Fig. 3. Yields *Y* of (*1*) liquid hydrocarbon product, (*2*) gases, (*3*) water, (*4*) naphtha fraction, (*5*) diesel fraction, and (*6*) heavy gas oil fraction as functions (a) of the catalyst operation time τ for the NiMo/WA-20 system and (b) of the WO_3 content of the support $c(WO_3)$.

to NiMo/WA-30 is similar, but the concentration of the radicals is 3–9 times lower compared to the initial support. A decrease in the BAS concentration correlates with the mechanism of adsorption of Ni^{2+} cations suggested in [56, 60] and based on the ion exchange involving surface BASs. As a result, the BAS concentration decreases.

Results of catalyst tests. A ^1H and ^{13}C NMR study of liquid products of sunflower oil conversion on NiMoS/WA catalysts has shown that, irrespective of the catalyst operation time (within 150 h), the products contained exclusively aliphatic hydrocarbons: linear and branched alkanes. Sulfur- and oxygen-containing compounds were not detected. Thus, the catalysts studied ensure complete hydrodeoxygenation of sunflower oil, and sulfur-containing compounds are not formed in the process, at least in amounts detectable by NMR.

Figure 3 shows how the yield of the major products depends on the catalyst operation time (with NiMoS/WA-20 catalyst as example, Fig. 3a) and how the time-averaged product yields depend on the tungsten oxide content of the support (Fig. 3b). To make the analysis of the results more convenient, the liquid hydrodeoxygenation products were conventionally subdivided into three fractions: naphtha (C_5–C_9), diesel (C_{10}–C_{20}), and C_{21+} fraction corresponding in the boiling range to heavy gas oil. As seen from Fig. 3a, the yields of the major products do not change significantly with time. In the first 4 h of the experiment, before the steady-state operation mode of the catalyst is reached, cracking reactions intensely occur, resulting in increased yield of the naphtha fraction and decreased yield of the diesel fraction. Apparently, the most active acid sites of the catalyst undergo deactivation in this period.

The yield of liquid hydrocarbons in all the systems is 81–83 wt %, which well agrees with the values calculated taking into account the initial oil composition: 81 wt % assuming that the whole amount of oxygen is removed in the form of CO and CO_2 and 86 wt % assuming that it is removed in the form of water. The diesel fraction yield is in the range 77–78 wt %, and the naphtha yield is 1–2 wt %. In the steady-state operation period, these yields are almost independent of the tungsten oxide content of the samples. The yield of the C_{21+} fraction is 1.8–2.7 wt %, appreciably exceeding the content of C_{22+} fatty acids in the initial oil (0.79). This fact can be attributed to the presence of oligomers in the initial oil. These oligomers undergo hydrodeoxygenation and cracking in the process, yielding C_{21+} products.

The yield of gaseous products does not exceed 16 wt %. The propane yield is 4.7–5.0 wt % for all the samples, which corresponds to the theoretical yield calculated for the case of complete hydrogenation of all the glycerol residues (5.0 wt %). Along with propane, the gas contains CO (yield 2–3 wt %), CO_2 (yield 3.5–4.5 wt %), and methane (yield less than 0.6 wt %).

Under the conditions of the experiment, such reactions as reduction of CO_2 to CO with hydrogen, hydrogenation of CO and CO_2 to methane, and oxidation of CO with water are possible. Therefore, it is impossible to determine from the composition of the gaseous products whether they were formed by decarbonylation/decarboxylation of fatty acids or by side reactions. However, comparison of the total molar yield of CO, CO_2, and CH_4 with the total yield of C_{15} and C_{17} hydrocarbons shows that their ratio for all the tungsten-containing catalysts is in the range 0.93–1.06, i.e., is very close to 1. This means that all the C_1 gases are formed by decarboxylation/decarbonylation of fatty acids. On the unmodified catalyst NiMoS/WA-0, the time-averaged value of this ratio is 1.38, indicating that this catalyst is more active in hydrogenolysis. This may be due to the presence of nickel in this catalyst not only as a component of NiMoS phases, but also in the metal form.

The influence of the support composition on the content of isoalkanes in the diesel fraction in relation to the catalyst operation time is shown in Fig. 4. As can be seen, the content of isoalkanes in the product obtained on the unmodified catalyst is 10 wt % in the initial period and decreases to 6–7 wt % over the course of 24 h. Introduction of tungsten oxide considerably enhances the catalyst activity in isomerization. The content of the isomers in the product correlates with the acidity of the samples and can reach 37 wt % in the initial time moments for the NiMoS/WA-25 sample. However, as in the case of the unmodified catalyst, the isomerizing ability of the samples strongly decreases in the first 48 h of their operation, after which the weight fraction of isoparaffins in the product does not exceed 7–10%. Thus, the acid sites of the catalysts undergo deactivation in the first 48 h of the operation.

Along with the isomeric composition of the diesel fraction, the sample acidity strongly influences the ratio of hydrocarbons with even and odd numbers of carbon atoms and hence the ratio of the rates of direct hydrodeoxygenation with the removal of water and decarboxylation/decarbonylation. The dependence of the ratio of the total yield of C_{15} and C_{17} hydrocarbons to the diesel fraction yield, $(C_{15} + C_{17})/\sum C_{15–18}$, on the catalyst operation time for samples with different tungsten oxide content is shown in Fig. 5.

As can be seen, this parameter depends on the support acidity and increases from 0.62 for NiMoS/WA-0 to 0.77 for NiMoS/WA-30 in the initial time moment. With time, the $(C_{15} + C_{17})/\sum C_{15–18}$ ratio monotonically decreases for all the samples, which, together with a decrease in the relative content of branched isomers in the products, suggests deactivation of acid sites of the catalyst.

CONCLUSIONS

(1) Modification of γ-alumina with tungsten oxide alters its textural characteristics. The samples containing 5–10 wt % WO_3 exhibit the maximal values of the pore volume and specific surface area.

(2) According to the data of TPD of ammonia and ESR of adsorbed perylene, the total amount of acid sites in WO_3–Al_2O_3 samples increases with an increase in the tungsten oxide content, and the distribution of acid sites changes: The content of weak and medium BASs increases, whereas the content of strong acid sites decreases compared to γ-Al_2O_3.

(3) The NiMoS/WO_3–Al_2O_3 catalysts, irrespective of the tungsten oxide content, allow complete hydrodeoxygenation of sunflower oil to obtain exclusively aliphatic hydrocarbons. The yield of liquid products in the process is 81–83 wt %.

(4) With an increase in the acidity of the WO_3–Al_2O_3 support, the fraction of isoparaffins in the products and the ratio of the decarboxylation/decarbonylation rate to direct hydrodeoxygenation rate increases. These parameters tend to decrease with the catalyst operation time because of deactivation of the acid sites.

ACKNOWLEDGMENTS

The physicochemical studies were performed using the scientific equipment of the Omsk Regional Center for Shared Use, Siberian Branch, Russian Academy of Sciences (Omsk).

REFERENCES

1. Choudhary, T.V. and Phillips, C.B., *Appl. Catal., Ser. A,* 2011, vol. 397, no. 1, pp. 1–12.
2. Mortensen, P.M., Grunwaldt, J.-D., Jensen, P.A., et al., *Appl. Catal., Ser. A*, 2011, vol. 407, no. 1, pp. 1–19.
3. Zhao, C., Bruck, T., and Lercher, J.A., *Green Chem*., 2013, vol. 15, no. 7, pp. 1720–1739.
4. Bengoechea, M.O., Hertzberg, A., Miletić, N., et al., *J. Anal. Appl. Pyrol*., 2015, vol. 113, pp. 713–722.

5. Herskowitz, M., Landau, M.V., Reizner, Y., and Berger, D., *Fuel,* 2013, vol. 111, pp. 157–164.
6. Veriansyah, B., Han, J.Y., Kim, S.K., et al., *Fuel*, 2012, vol. 94, pp. 578–585.
7. De Sousa, F.P., Cardoso, C.C., and Pasa, V.M.D., *Fuel Process. Technol*., 2016, vol. 143, pp. 35–42.
8. Kubička, D. and Kaluža, L., *Appl. Catal., Ser. A*, 2010, vol. 372, no. 2, pp. 199–208.
9. Besenbacher, F., Bronson, M., and Clausen, B.S., *Catal. Today*, 2008, vol. 130, pp. 86–96.
10. Kubička, D. and Horáček, J., *Appl. Catal., Ser. A*, 2011, vol. 394, no. 1, pp. 9–17.
11. Krár, M., Kovács, S., Kalló, D., and Hancsók, J., *Bioresource Technol*., 2010, vol. 101, no. 23, pp. 9287–9293.
12. Hancsók, J., Kasza, T., Kovács, S., et al., J. *Cleaner Prod.,* 2012, vol. 34, pp. 76–81.
13. Kordouli, E., Sygellou, L., Kordulis, C., et al., *Appl. Catal., Ser. B*, 2017, vol. 209, pp. 12–22.
14. Bie, Y., Lehtonen, J., and Kanervo, *J., Appl. Catal., Ser. A*, 2016, vol. 526, pp. 183–190.
15. Gutierrez, A., Turpeinen, E.-M., Viljava, T.-R., and Krause, O., *Catal. Today*, 2017, vol. 285, pp. 125–134.
16. Gusmao, J., Brodzki, D., Djéga-Mariadassou, G., and Frety, R., *Catal. Today*, 1989, vol. 5, no. 4, pp. 533–544.
17. Guzman, A., Torres, J.E., Prada, L.P., and Nunez, M.L., *Catal. Today*, 2010, vol. 156, nos. 1–2, pp. 38–43.
18. Da Rocha Filho, G., Brodzki, D., and Djéga-Mariadassou, G., *Fuel*, 1993, vol. 72, no. 4, pp. 543–549.
19. Huber, G.W., O'Connor, P., and Corma, A., *Appl. Catal., Ser. A*, 2007, vol. 329, no. 1, pp. 120–129.
20. Šimáček, P., Kubička, D., Šebor, G., and Pospíšil, M., *Fuel*, 2009, vol. 88, no. 3, pp. 456–460.
21. Patent WO 2013050653 A1, Publ. 2013.
22. Patent EP 1 728 844 A1, Publ. 2006.
23. Brillouet, S., Baltag, E., Brunet, S., and Richard, F., *Appl. Catal., Ser. B*, 2011, vols. 148–149, pp. 201–211.
24. Wagenhofer, M.F., Barath, E., Gutierrez, O.Y., and Lercher, J.A., *ACS Catal*., 2017, vol. 7, no. 2, pp. 1068−1076.
25. Şenol, O.I., Ryymin, E.-M., Viljava, T.-R., and Krause, A.O.I., *J. Mol. Catal., Ser. A*, 2007, vol. 277, nos. 1–2, pp. 107–112.
26. Coumans, A.E. and Hensen, E.J.M., *Appl. Catal., Ser. B*, 2017, vol. 201, pp. 290–301.
27. Kubička, D., Horáček, J., Setnička, M., et al., *Appl. Catal., Ser. B*, 2014, vol. 145, pp. 101–107.
28. Qian, E.W., Chen, N., and Gong, S., J. *Mol. Catal., Ser. A*, 2014, vol. 387, pp. 76–85.
29. Madsen, A.T., Ahmed, E.H., Christensen, C.H., et al., *Fuel,* 2011, vol. 90, no. 11, pp. 3433–3438.
30. Zarchin, R., Rabaev, M., Vidruk-Nehemya, R., et al., *Fuel*, 2015, vol. 139, pp. 684–691.
31. Yang, Y., Wang, Q., Zhang, X., et al., *Fuel Process. Technol*., 2013, vol. 116, pp. 165–174.
32. Sagata, K., Hirose, M., Hirano, Y., and Kita, Y., *Appl. Catal., Ser. A*, 2016, vol. 523, pp. 85–91.
33. Santillan-Jimenez, E., Morgan, T., Lacny, J., et al*., Fuel*, 2013, vol. 103, pp. 1010–1017.
34. Yasir, M., Azizan, M.T., Ramli, A., and Ameen, M., *Procedia Eng*., 2016, V. 148. P. 275–281.
35. Mikulec, J., Cvengroš, J., Joríková, L., et al., *J. Cleaner Prod*., 2010, vol. 18, no.. 9, pp. 917–926.
36. Mortensen, P.M., de Carvalho, H.W.P., Grunwaldt, J.-D., et al., *J. Catal*., 2015, vol. 328, pp. 208–215.
37. Bui, V.N., Laurenti, D., Delichere, P., and Geantet, C., *Appl. Catal., Ser. B*, 2011, vol. 101, nos. 3–4, pp. 246–255.
38. Duan, J., Han, J., Sun, H., et al., *Catal. Commun*., 2012, vol. 17, pp. 76–80.
39. Kubička, D., Bejblová, M., and Vlk, J., *Top. Catal*., 2010, vol. 53, pp. 168–178.
40. Wang, C., Liu, Q., Song, J., et al., *Catal. Today*, 2014, vol. 234, pp. 153–160.
41. Liu, Q., Zuo, H., Zhang, Q., et al., *Cuihua Xuebao/Chin. J. Catal*., 2014, Vol. 35, no. 5, pp. 748–756.
42. Chen, N., Gong, S., and Qian, E.W., *Appl. Catal., Ser. B*, 2015, vols. 174–175, pp. 253–263.
43. Liu, Q., Zuo, H., Wang, T., et al., *Appl. Catal., Ser. A*, 2013, vol. 468, pp. 68–74.
44. Shahinuzzaman, M., Yaakob, Z., and Ahmed, Y., *Renew. Sustain. Energy Rev*., 2017, vol. 77, pp. 1375–1384.
45. Ishihara, A., Fukui, N., Nasu, H., and Hashimoto, T., *Fuel*, 2014, vol. 134, pp. 611–617.
46. Toba, M., Abe, Y., Kuramochi, H., et al., *Catal. Today*, 2011, vol. 164, no. 1, pp. 533–537.
47. Chumachenko, Yu.A., Lavrenov, A.V., Buluchevskii, E.A., et al., *Katal. Prom–sti*., 2015, vol. 15, no. 4, pp. 49–64.
48. Mohammad, M., Kandaramath Hari, T., and Yaakob, Z., *Renew. Sustain. Energy Rev*., 2013, vol. 22, pp. 121–132.
49. Patent WO 2004022674 A1, Publ. 2004.
50. Patent EP 1396531 B2, Publ. 2004.
51. Tom, N., Kalnes, T., Marker, T., et al., *Biofuels Technol*., 2008, Q4, pp. 7–11.
52. Kikhtyanin, O.V., Rubanov, A.E., Ayupov, A.B., and

Echevsky, G.V., *Fuel*, 2010, vol. 89, pp. 3085–3092.

53. Choi, I.H., Hwang, K.R., Han, J.S., et al., *Fuel*, 2015, vol. 158, pp. 98–104.
54. Liu, S., Zhu, Q., Guan, Q., et al., *Bioresource Technol*., 2015, vol. 183, pp. 93–100.
55. Wang, C., Tian, Z., and Wang, L., *ChemSusChem*, 2012, vol. 5, no. 10, pp. 1974–1983.
56. Yurpalov, V.L., Drozdov, V.A., Karpova, T.R., and Lavrenov, A.V., *Chem. Sustain. Develop.*, 2017, vol. 25, no. 1, pp. 107–113.
57. *Khimicheskaya entsiklopediya* (Chemical Encyclopedia), Knunyants, I.L., Ed., Moscow: Sov. Entsiklopediya, 1988, vol. 1, p. 421.
58. Shannon, R.D., *Acta Crystallogr., Sect. A*, 1976, vol. 32, pp. 751–767.
59. Fedorova, E.D., Kazakov, M.O., Lavrenov, A.V., et al., *Chem. Sustain. Develop*., 2013, vol. 21, no. 1, pp. 107–113.
60. Karpova, T.R., Lavrenov, A.V., Buluchevsky, E.A., et al., *Catal. Ind*., 2014, vol. 6, no. 2, pp. 105–113.